Proceedings of the 5th World Congress on Momentum, Heat and Mass Transfer (MHMT'20)
~~Lisbon, Portugal~~ Virtual Conference– October, 2020
Paper No. ICMFHT 147
DOI: 10.11159/icmfht20.147

Effect of Channel Aspect Ratio on Flow Boiling Characteristics within Rectangular Micro-passages

Manolia Andredaki[1], Konstantinos Vontas[1], Anastasios Georgoulas[1], Nico Miché[1] and Marco Marengo[1]
[1]Advanced Engineering Centre, School of Computing Engineering and Mathematics, University of Brighton
Lewes Road, BN2 4GJ, Brighton, East Sussex, U.K
m.andredaki@brighton.ac.uk; k.vontas@brighton.ac.uk; a.georgoulas@brighton.ac.uk; n.d.d.miche@brighton.ac.uk; m.marengo@brighton.ac.uk

Abstract **-** A numerical investigation on the effect of channel aspect ratio on a single bubble growth during saturated flow boiling conditions within square microchannels, is conducted in the present paper. The open-source toolbox OpenFOAM is applied for the simulations, utilising a user-enhanced Volume OF Fluid (VOF) solver. The solver enhancements include a treatment for spurious velocities dampening, the implementation of an improved dynamic contact angle sub-model for accurate prediction of wettability effects as well as the implementation of a phase-change model in the fluid domain, accounting for conjugate heat-transfer with a solid domain. It is shown that the variation of the aspect ratio of a microchannel has a significant effect in the local heat transfer coefficient, due to an enhancement of the single-phase heat transfer in combination with the alteration of the underpinned bubble growth dynamics, which result in different contributions of contact line versus liquid film evaporation.

Keywords**:** Flow boiling, Microchannels, Multiphase flow, VOF, Conjugate heat transfer

1. Introduction

Due to the continuously increasing performance requirements and miniaturisation trends of micro-electronic components such as computer chips and high-power electronics, their efficient thermal management has become a challenging issue. It has been reported [1] that by 2026, the average heat flux that needs to be dissipated from computer chips is expected to reach values in the range of 2-4.5 MW/m^2. Similarly, Insulated Gate Bipolar Transistor (IGBT) modules, at the chip level, might reach heat flux values in the range of 6.5-50 MW/m^2. Conventional cooling methods, such as air cooling or pumped liquid cooling, cannot cope with such high heat dissipation demands. Flow boiling heat transfer within microchannels has been recognised experimentally as one of the most efficient thermal management solutions for such high-power density electronic components, dissipating heat fluxes in the order of MW/m^2 [2]. However, cooling of micro-electronics utilising flow boiling within micro-passages is not yet commercially available and it is still limited to laboratory applications. The main reason for this, is the lack of accurate design correlations as well as the lack of understanding of several underpinned principles and mechanisms. Karayiannis and Mahmoud [3] recently reported the still open fundamental research aspects and issues. One of these open research aspects is the effect of channel geometry. In particular, in the case of rectangular micro-channels, the developed flow patterns, the heat transfer mechanisms and rates as well as the encountered pressure drops, can be affected by the aspect ratio of the channel cross-section, defined as the ratio of the channel width over the channel height (β=W/H). Soupremanien et al. [4] used Forane 365HX in two stainless steel channels of hydraulic diameter 1.4 mm and β = 2.3 and 7, respectively. They found that at low heat flux, the heat transfer coefficient was higher for the channel of β = 7 but the trend is reversed at higher values of heat flux. Fu et al. [5] carried out flow boiling experiments with HFE-7100 in a diverging copper channel of hydraulic diameter approximately 1.12 mm and aspect ratios β ranging from 0.16 to 1.2. They noted a significant aspect ratio effect with a maximum heat transfer coefficient at β = 1.01. Markal et al. [6] examined the effect of aspect ratio testing six silicon heat sinks 48 mm long and 13.5 mm wide that consisted of 29 rectangular channels of the same hydraulic diameter (D_h=0.1 mm) and aspect ratio values ranging from 0.37 to 5.0. It was found that the heat transfer coefficient increases with increasing aspect ratio up to β = 3.54 and then decreases with further increase of β. Summarising, from the variety of different conclusions withdrawn from these previous experimental investigations, it is evident that further studies are needed in this direction that must examine the effect of channel aspect ratio for a range of heat fluxes and mass fluxes. Moreover, despite the wide number of experimental investigations, in most cases unavoidable differences on factors such as the surface roughness of the examined channels, might lead to misleading conclusions. From another point of view, with the advances in the available numerical simulation techniques in the last

decades, and the availability of significant computational resources, the direct numerical simulation of two-phase flows with interface-capturing methods can provide valuable information on the underpinned bubble dynamics and heat transfer mechanisms, for cases of flow boiling within micro-passages. The present numerical investigation aims to isolate, identify and quantify the effect of channel aspect ratio on the transient local bubble growth and heat transfer characteristics, by simulating the behaviour of an isolated bubble nucleus that grows within microchannels of the same hydraulic diameter (D_h = 0.2 mm) but with three different values of aspect ratio (β = 0.5, 1.0 and 2.5), in saturated flow boiling conditions. The same channels are examined for three different values of applied heat flux (q''=20, 50, 100 KW/m^2). It should be highlighted that conjugate heat transfer between the fluid and solid domains is considered, in order to account for the solid channel wall thermal inertia.

2. Numerical Method

2.1. Governing Equations

The numerical simulations of the present paper are conducted with the open-source toolbox OpenFOAM, utilising a user-enhanced Volume OF Fluid (VOF) solver. The proposed solver enhancements involve a treatment for spurious velocities dampening (a well-known defect of VOF methods), an improved dynamic contact angle treatment to accurately account for wettability effects as well as the implementation of a phase-change model in the fluid domain, accounting for conjugate heat-transfer with a solid domain. In this section, the governing equations for mass, momentum, energy, and volume fraction are presented. The liquid and vapour phases are both treated as incompressible, Newtonian fluids. This solver has been extensively validated in the past against various cases of adiabatic and diabatic bubble and droplet dynamics in comparison with available analytical solutions as wells as experimental measurements. Further details can be found in [7]–[10].

The mass conservation equation is given as:

$$\nabla \cdot \left(\rho \vec{U}\right) = \dot{\rho} \tag{1}$$

where $\vec{U}$ is the fluid velocity and ρ is the bulk density. The source term on the right-hand side $\dot{\rho}$ accounts for the phase change. The conservation of momentum is given by the following equation:

$$\frac{\partial}{\partial t}\left(\rho \vec{U}\right) + \nabla \cdot \left(\rho \vec{U}\vec{U}\right) - \nabla \cdot \left\{\mu\left[\nabla \vec{U} + \left(\nabla \vec{U}\right)^T\right]\right\} = -\nabla p + \vec{f}_{ST} + \vec{f}_g \tag{2}$$

where p is the pressure and μ is the bulk dynamic viscosity. The momentum source terms on the right-hand side of the equation account for the effects of surface tension ($\vec{f}_{ST}$) and gravity($\vec{f}_g$), respectively. The surface tension term is modelled according to the classical approach of Brackbill et al. [11]. The conservation of energy balance in the fluid domain is given by the following equation:

$$\frac{\partial}{\partial t}\left(\rho c_p T\right) + \nabla \cdot \left(\vec{U}\rho c_p T\right) - \nabla \cdot \left(\lambda \nabla T\right) = \dot{h} \tag{3}$$

where c_p is the bulk heat capacity, T the temperature field, and λ is the bulk thermal conductivity. The source term on the right-hand side of the equation ($\dot{h}$) represents the contribution of the enthalpy of evaporation/condensation or else the cooling/heating associated with the latent heat of the phase-change. The volume fraction α is advected by the flow field by the following equation:

$$\frac{\partial \alpha}{\partial t} + \nabla \cdot \left(\alpha \vec{U}\right) - \nabla \cdot \left(\alpha(1-\alpha)\vec{U}_r\right) = \frac{\dot{\rho}}{\rho}\alpha \tag{4}$$

Interface sharpening is very important in simulating two-phase flows of two immiscible fluids. In OpenFOAM the sharpening of the interface is achieved artificially by introducing the extra compression term $\nabla \cdot \left(\alpha(1-\alpha)\vec{U}_r\right)$ in Equation (4). $\vec{U}_r$ is an artificial compression velocity. The source term on the right-hand side of the Equation (4) flows $(\frac{\dot{\rho}}{\rho}\alpha)$ is needed because, due to the local mass source terms, the velocity field is not free of divergence. Finally, the bulk fluid properties γ are computed as the averages over the liquid (γ_l) and vapour (γ_v) phases, weighted with the volume fraction α, i.e. $\gamma=\alpha\gamma_l+(1-\alpha)\gamma_v$. S mentioned previously, the VOF-based solver that is used in the present investigation has been modified accordingly in order to account for an adequate level of spurious currents suppression. More details on the proposed development and validation as well as on the proposed improved VOF method can be found in the paper by Georgoulas et al [7].

The conservation of energy equation in the solid domains is defined as:

$$\frac{\partial}{\partial t}\left(\rho_s c_{ps} T\right) = \nabla \cdot (\lambda_s \nabla T) \tag{5}$$

Where ρ_s and c_{ps} are the solid density and heat capacity respectively. The coupling at the interface between the solid and fluid region is achieved iteratively through the following conditions:

$$T_f = T_s \lambda_f \, , \frac{\partial T_f}{\partial n} = \lambda_s \frac{\partial T_s}{\partial n} \tag{6}$$

where T_f is the temperature at the fluid side and T_s is the temperature at the solid side of the conjugate heat transfer boundary, λ_f is the thermal conductivity of the fluid domain and λ_s is the thermal conductivity of the solid domain.

2.2. Phase Change Model

The phase change model originally proposed by Hardt and Wondra [12] has been implemented in the improved OpenFOAM VOF solver that is used in the present investigation. Further details on the proposed development and validation can be found in the work of Georgoulas et al. [13].

2.3. Dynamic Contact Angle Treatment

The utilised numerical simulation model includes also an implementation of the dynamic contact angle (DCA) model originally suggested by Kistler [14]. This implementation has been validated in the past against experiments available in the literature for droplet impact on flat surfaces with different wettability [15] as well as against experiments of pool boiling in biphilic surfaces [16].

3. Application of Numerical Model

3.1. Computational Geometry, Mesh and Boundary Conditions

In Fig. 1(a) the generated computational geometry, mesh and the applied boundary conditions are illustrated indicatively for β =0.5. As it can be seen the computational mesh has been generated by discretising the computational domain in two parts. The solid domain and the fluid domain. A uniform, structured computational mesh, consisting of hexahedral elements is utilised. After a mesh independence study, an element size of 2μm was selected. The total number of cells for the solid domain is 2.025M and 6.75M for the fluid domain. The fluid domain dimensions (length, height and width) are L_f = 2.4 mm, H_f = 0.30 mm, W_f = 0.15 mm and the solid domain dimensions are L_s = 2.4 mm, H_s = 0.09 mm, W_s = 0.15 mm. For the geometry with β =1.0 the fluid and solid domain dimensions are L_f = 2.4 mm, H_f = 0.20 mm, W_f = 0.20 mm and L_s = 2.4 mm, H_s = 0.09 mm, W_s = 0.2 mm (the total number of cells for the solid domain is 5.40M and 12.00M for the fluid domain, in this case). For the geometry with β =2.5 the fluid and solid domain dimensions are L_f = 2.4 mm, H_f = 0.14 mm, W_f = 0.35 mm and L_s = 2.4 mm, H_s = 0.09, W_s = 0.35 mm (the total number of cells for the solid domain is 9.45M and 14.70M for the fluid domain, in this case). For all cases considered, except from the inlet and outlet in the fluid domain and the bottom side of the solid domain, where a constant heat flux is applied, all the rest surfaces are considered to be adiabatic walls. At the solid walls, a no-slip velocity boundary condition was used with a fixed flux pressure boundary condition for the pressure values. Moreover, a dynamic contact angle boundary condition is imposed for the volume fraction field by

assigning the maximum advancing and minimum receding contact angle values from sessile drop measurements, that are then used for the calculation of the dynamic apparent contact angle values during the computations. For the sidewalls of the fluid and solid domains, a zero gradient boundary condition was used for the temperature field. At the outlet, a fixed-value pressure boundary condition and a zero-gradient boundary condition for the volume fraction were used, while for the velocity values a special (combined) type of boundary condition was used that applies a zero-gradient when the fluid mixture exits the computational domain and a fixed value condition to the tangential velocity component, in cases that the fluid mixture enters the domain. Finally, a zero gradient boundary condition for the temperature field was also prescribed at the outlet boundary. For the inlet, a constant uniform velocity value was imposed as well as a fixed flux pressure condition. The volume fraction value was assigned as unity, as saturated liquid only enters from the inlet during the calculations. Hence, the temperature of the liquid at the inlet was also fixed at the saturation temperature. As mentioned earlier both the temperature values as well as the heat fluxes are coupled at the conjugate heat transfer interface, for each calculation time step, through an inner iteration process.

3.2. Numerical Simulation Set-up and Process

All the simulations are performed in two main stages. During the first stage a specified heat flux is applied to the bottom surface of the solid domain, and a single-phase liquid flow is considered initially with saturated liquid flowing with a specified mass flow rate. This is run up to a point that a steady state condition is reached and both the hydrodynamic and thermal boundary layers, have been developed. The velocity of the liquid $U_{l\ is}$ constant and uniform through the inlet boundary and the flow is laminar. At the second stage a small vapour nucleus (bubble seed) represented as a half-sphere with a radius of 20 μm is patched on the conjugate heat transfer boundary (interface between the fluid and liquid domains) at a distance of 200 μm from the channel inlet, at saturation temperature. Since this initial bubble seed is patched within the previously developed thermal boundary layer where the temperature is higher than the saturation temperature, boiling occurs at the meniscus (solid/liquid/vapour triple line) as well as at the parts of the liquid/vapour interface away from the heated wall that are in contact with temperatures higher that the saturation temperature. It should be mentioned that for all of the simulations conducted for the present investigation the liquid and vapour phase properties are taken as these of Ethanol liquid and vapour at the saturation equilibrium point for a pressure of P_{sat} = 1 bar, which corresponds to a saturation temperature of T_{sat} = 351.05 K (REFPROP NIST software). Hence, the liquid and vapour densities where taken as ρ_l = 736.78 kg/m^3 and ρ_v = 1.63 kg/m^3, the liquid and vapour kinematic viscosities as $\nu_l = 6.01 \times 10^{-7}$ m^2/s and $\nu_v = 6.37 \times 10^{-6}$ m^2/s, the liquid and vapour thermal conductivities as λ_l = 0.15 W/mK and λ_v = 0.02 W/mK and the liquid and vapour heat capacities as $c_{p,l}$= 3182 J/kgK and $c_{p,v}$= 1804 J/kgK. For the solid domain stainless steel properties are used. In more detail the density of the solid domain is taken as ρ = 7840 kg/m^3, the specific heat as $c_{v,s}$ = 500 J/kgK and the thermal conductivity as λ_s = 16.2 W/mK. The advancing (θ_a) and receding (θ_r) contact angles were taken as these of Ethanol with a particular stainless-steel sample with roughness Ra=0.4 μm, having values of 19º and 18º, respectively. In order to observe the effects of channel aspect ratio at different heat fluxes, the overall analysis for all of the considered channel cross-sections was performed for three different values of applied heat flux (q''=20, 50, 100 KW/m^2). In order to maintain the same total power to mass flow rate ratio (since the width of the channel is changing and the applied heat flux is kept constant) a slightly different mass flow rate was applied for the different channel aspect ratios. The overall details regarding the different channel aspect ratio cases considered for each of the examined applied heat flux values are summarised in Table 1. Therefore, nine, 3D, transient, two-phase numerical simulations were performed. For each of these cases, as mentioned earlier a single-phase simulation was initially run in order for the hydrodynamic and thermal boundary layers to be developed reaching a steady state condition. Therefore, the total number of simulations that were performed for the present investigation were 18. A High-Performance Computing (HPC) cluster was utilised for these runs. Each run required 200 computational cores. The duration of the computation for each of the nine single phase simulations (one for each q'' value) was approximately 10 days, as seconds of real flow were required for a steady state condition to be reached. For the two-phase simulations the duration of the computation was only a couple of days since just a few milliseconds of real flow where required for the generated vapour bubble to reach the outlet of the channel. In total 518,400 core-hours were utilized for the final runs that are presented in the paper. A variable calculation time step was utilised for the two-phase runs with the courant number kept constant at 0.5. Hence the calculation time step was varied automatically ranging from 10^{-8} up to 10^{-6} s.

Table 1: Considered channel cross-sections and corresponding mass flow rates (these cases are considered for q″=20, 50, 100 KW/m^2).

Case	W (mm)	*H (mm)*	D_h *(mm)*	*β (mm)*	$\dot{m}$ *(kg/m^{2}s)*	U_l *(m/s)*
I	0.15	0.30	0.20	0.5	150	0.203
II	0.20	0.20	0.20	1.0	133	0.180
III	0.35	0.14	0.20	2.5	163.3	0.221

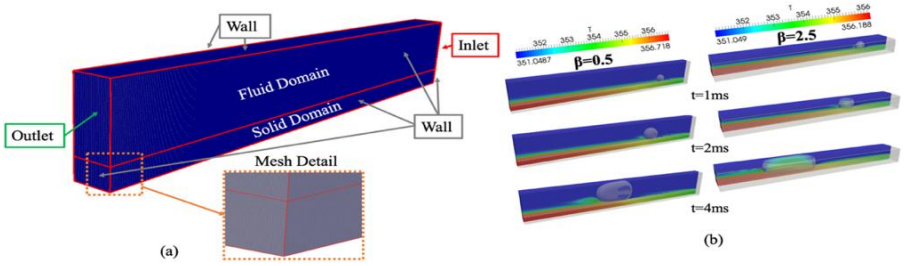

Fig. 1: (a) Computational domain, boundary conditions and mesh details. (b) Spatial and temporal evolution of the generated vapour bubble for q'' = 20kW/m^2 and for aspect ratio cases I and III (please see Table 1).

4. Numerical Simulation Results

The spatial and temporal evolution of the generated vapour bubble for Cases I and III for an applied heat flux value of q'' = 20kW/m^2, is depicted in Fig. 1(b). The grey surface represents the liquid/vapour interface, while the coloured contours in a clip section that extends from one side of the channel up to its middle plane, reveal the developed temperature fields in both the fluid and solid regions of the computational domain. It is evident that the variation of the channel aspect ratio has a quite significant effect in the resulting bubble growth dynamics. For β = 0.5, the bubble grows into a Taylor bubble maintaining minimal contact with the channel walls, with a liquid film formed between the bubble and the channel walls, apart from some small dry patches. For β = 2.5, the bubble grows into an elongated vapour slug that maintains contact with the top and bottom walls of the channel throughout the majority of its length. In the first case the bubble grows mainly due to liquid film evaporation, while in the second case the bubble grows due to vapour/liquid/solid contact line evaporation. Moreover, in both cases due to the associated latent heat of evaporation as the bubble grows and moves towards the outlet, the temperature at the heated solid domain is decreasing. However, in order to identify and quantify the effects of channel aspect ratio on the local instantaneous heat transfer, in Figs. 2, 3 and 4 the Nusselt number Nu is plotted over the dimensionless length L* = L(x) / L_{max} of the considered microchannel, along the central longitudinal axis of the conjugate heat transfer boundary, for the three considered channel aspect ratios and for each value of the applied heat flux, respectively. In each figure the resulting curves for three successive time instances after the bubble nucleation are shown. In all cases also the corresponding single-phase curve is plotted as a reference. Finally, the temporal and spatial bubble evolution is also shown for each case (as in Fig. 1(b)). The local heat transfer coefficient is calculated as the ratio of the applied heat flux over the temperature difference between the heated wall temperature and the saturation temperature ($h=q''/T_w-T_s$) and Nu is calculated as the ratio of the product of the local heat transfer coefficient with the channel hydraulic diameter over the thermal conductivity of the liquid ($Nu=hD_h/\lambda_l$). First of all, focusing on the single-phase curves it can be observed that the initial increase of β from 0.5 to 1.0, results in slightly lower values of Nu along the heated wall. However, the further increase of β to 2.5 results in a significant increase in the values of Nu, indicating an enhancement in the local heat transfer coefficient. Now examining the two-phase curves, it can be observed, that for all three values of the applied heat flux, at the early stages of the bubble growth (time t = 1.0 ms for q'' = 20 kW/m^2, t = 0.5 ms for q'' = 50 kW/m^2 and t = 0.2 ms for q'' = 100 kW/m^2), two successive peaks in the Nu number are encountered in comparison with the corresponding single-phase curves. These are due to the contact line evaporation at these points along the channel wall. As the bubble growth process continues (time t = 2.0 ms for q'' = 20 kW/m^2, t = 1.0 ms for q'' = 50 kW/m^2 and t = 0.6 ms for q'' = 100 kW/m^2), for the β = 0.5 channel, where the bubble maintains a minimal contact area with the heated wall with a successively developing liquid film region, the local heat transfer is significantly enhanced due to liquid film evaporation, approaching Nu values similar to the β = 2.5 case. In this case it is characteristic that an enhanced local heat transfer zone is traced also upstream of the bubble position that gradually attenuates with distance towards the inlet of the channel. As for cases with β = 1.0 and 2.5, where the growing

bubbles maintain a significant contact area with the heated wall of the channel, local increase of the Nu number (with respect to the single-phase curves) is observed at the points where the central wall longitudinal axis (sampling line) meets the contact line between the bubble interface and the heated wall. Also in these cases, upstream of the first peak point an enhanced region of local heat transfer is traced that gradually attenuates to the single-phase values towards the inlet. This is due to the thermal inertia of the solid domain. In more detail, in general as the bubble grows and moves towards the exit of the channel, due to either contact line evaporation or liquid film evaporation or due to a combination of these two mechanisms, the solid wall temperature is reduced significantly, resulting to an increase in the local heat transfer coefficient. However, due to the thermal inertia of the solid wall, it takes some time for the wall temperature to increase again, resulting in this region of enhanced local heat transfer, behind the moving bubbles. The same behaviour is observed also for the later stages of the bubble growth process (time t = 5.0 ms for q'' = 20 kW/m^2, t = 2.0 ms for q'' = 50 kW/m^2 and t = 0.9 ms for q'' = 100 kW/m^2). However, for q'' = 100 kW/m^2, liquid films have been developed for all three β cases, leading to a significant enhancement of the local heat transfer. From all these observations it is evident that the variation of the aspect ratio of a microchannel has a significant effect in the local heat transfer coefficient due to an enhancement in the single-phase heat transfer, combined with the alteration of the underpinned bubble growth dynamics that may result in different contributions of contact line versus liquid film evaporation. Furthermore, it is shown that the thickness and thermal properties of the channel walls have a major impact on the local heat transfer, due to the associated thermal inertia of the solid domains.

5. Conclusions

In the present paper, a parametric numerical investigation has been performed aiming to identify and quantify the effect of channel aspect ratio in the bubble growth characteristics for the case of isolated bubbles growing within heated rectangular microchannels. From the overall analysis and presentation of the results, it can be concluded that for the considered flow rate and applied heat fluxes, the effect of the aspect ratio in the local heat transfer coefficient is quite significant. In more detail the overall resulting effect is a combination of single phase heat transfer enhancement with the alteration of the underpinned bubble growth dynamics that result in different contributions of contact line versus liquid film evaporation. It is also found that the thickness and thermal properties of the channel walls have a major impact on the overall heat transfer enhancement, due to the associated thermal inertia of the solid material. This highlights the importance of coupled conjugate heat transfer simulations between fluid and solid regions in studies of flow boiling heat transfer within micro-passages. For future investigations, different flow rates and working fluids need to be tested, to further quantify the examined effect.

Acknowledgements

This research was partially funded through the European Union's Horizon 2020 research and innovation programme (Marie Skłodowska Curie grant agreement No 801604), the UK's Engineering and Physical Science Research Council (grant EP/P013112/1), and the European Space Agency (ESA MAP CORA projects TOPDESS and ENCOM4).

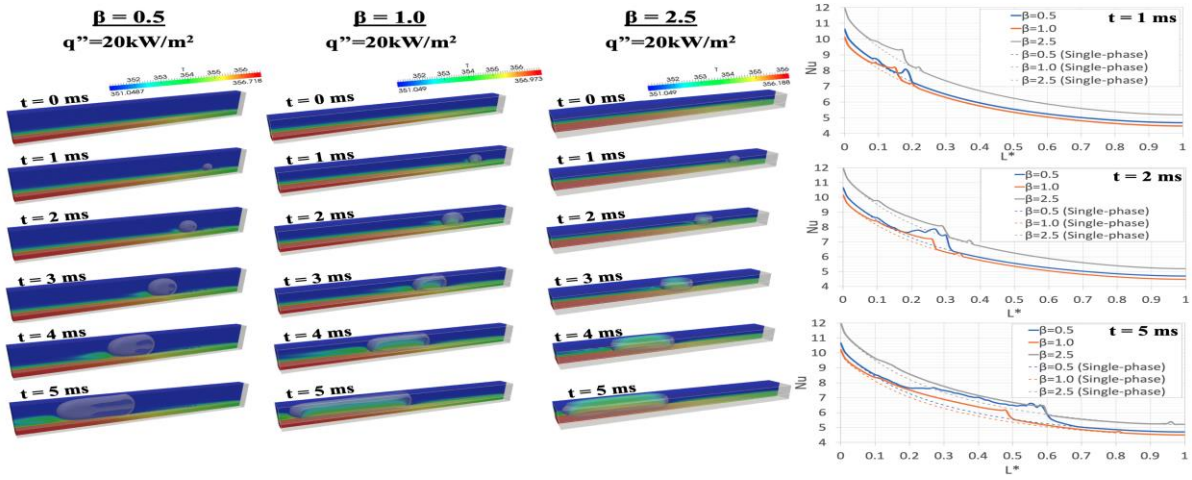

Fig. 2: Effect of β on the local Nusselt number along the heated wall as a function of dimensionless length (q'' = 20 kW/m^2).

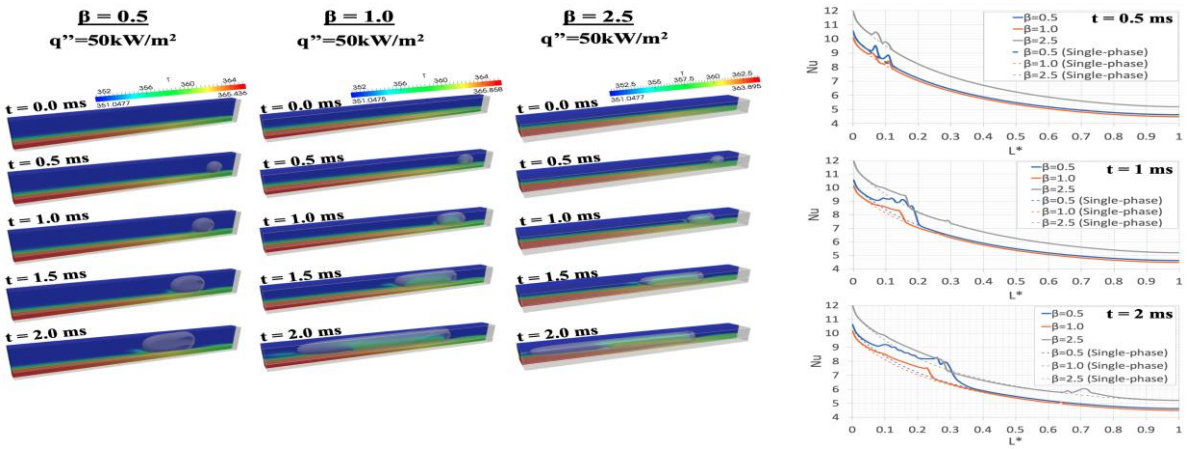

Fig. 3: Effect of β on the local Nusselt number along the heated wall as a function of dimensionless length (q'' = 50 kW/m^2).

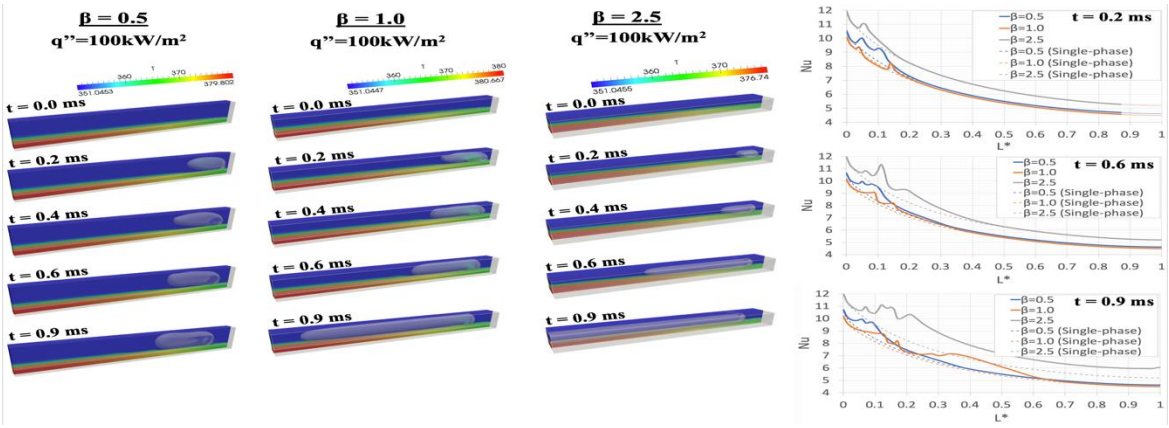

Fig. 4: Effect of β on the local Nusselt number along the heated wall as a function of dimensionless length (q'' = 100 kW/m^2).

References

[1] T. G. Karayiannis and M. M. Mahmoud, "Flow boiling in microchannels: Fundamentals and applications," Appl. Therm. Eng., vol. 115, pp. 1372–1397, Mar. 2017.

[2] K. P. Drummond, D. Back, M. D. Sinanis, D. B. Janes, D. Peroulis, J. A. Weibel and S. V. Garimela, "A hierarchical manifold microchannel heat sink array for high-heat-flux two-phase cooling of electronics," Int. J. Heat Mass Transf., vol. 117, pp. 319–330, Feb. 2018.

[3] T. G. Karayiannis and M. M. Mahmoud, "FLOW BOILING IN MICRO-PASSAGES: DEVELOPMENTS IN FUNDAMENTAL ASPECTS AND APPLICATIONS," in 16th International Heat Transfer Conference, IHTC-16, 2018.

[4] U. Soupremanien, S. Le Person, M. Favre-Marinet, and Y. Bultel, "Influence of the aspect ratio on boiling flows in rectangular mini-channels," Exp. Therm. Fluid Sci., vol. 35, no. 5, pp. 797–809, Jul. 2011.

[5] B. R. Fu, C. Y. Lee, and C. Pan, "The effect of aspect ratio on flow boiling heat transfer of HFE-7100 in a microchannel heat sink," Int. J. Heat Mass Transf., vol. 58, no. 1–2, pp. 53–61, Mar. 2013.

[6] B. Markal, O. Aydin, and M. Avci, "Effect of aspect ratio on saturated flow boiling in microchannels," Int. J. Heat Mass Transf., vol. 93, pp. 130–143, Feb. 2016.

[7] A. Georgoulas, P. Koukouvinis, M. Gavaises, and M. Marengo, "Numerical investigation of quasi-static bubble growth and detachment from submerged orifices in isothermal liquid pools: The effect of varying fluid properties and gravity

levels," Int. J. Multiph. Flow, vol. 74, pp. 59–78, 2015.
[8] A. Georgoulas, M. Andredaki, and M. Marengo, "An Enhanced VOF Method Coupled with Heat Transfer and Phase Change to Characterise Bubble Detachment in Saturated Pool Boiling," Energies, vol. 10, no. 3, p. 272, Feb. 2017.
[9] E. Teodori, P. Pontes, A. Moita, A. Georgoulas, M. Marengo, and A. Moreira, "Sensible heat transfer during droplet cooling: Experimental and numerical analysis," Energies, vol. 10, no. 6, 2017.
[10] K. Vontas, M. Andredaki, A. Georgoulas, K. S. Nikas, and M. Marengo, "Numerical Investigation of Droplet Impact on Smooth Surfaces with Different Wettability Characteristics: Implementation of a dynamic contact angle treatment in OpenFOAM," in 28th European Conference on Liquid Atomization and Spray Systems, 2017.
[11] J. Brackbill, D. Kothe, and C. Zemach, "A continuum method for modeling surface tension," J. Comput. Phys., vol. 100, no. 2, pp. 335–354, Jun. 1992.
[12] S. Hardt and F. Wondra, "Evaporation model for interfacial flows based on a continuum-field representation of the source terms," J. Comput. Phys., vol. 227, no. 11, pp. 5871–5895, 2008.
[13] A. Georgoulas, M. Andredaki, and M. Marengo, "An enhanced VOF method coupled with heat transfer and phase change to characterise bubble detachment in saturated pool boiling," Energies, vol. 10, no. 3, 2017.
[14] S. F. Kistler, "In Hydrodynamics of Wetting," in Wettability, no. 1993, J. C. Berg, Ed. (Dekker, New York, 1993), pp. 311-429, 1993.
[15] K. Vontas, M. Andredaki, A. Georgoulas, K. S. Nikas, and M. Marengo, "Numerical Investigation of Droplet Impact on Smooth Surfaces with Different Wettability Characteristics: Implementation of a dynamic contact angle treatment in OpenFOAM.," Proc. ILASS–Europe 2017. 28th Conf. Liq. At. Spray Syst., no. September, pp. 6–8, 2017.
[16] P. Pontes, R. Cautela, E. Teodori, A. Moita, A. Georgoulas, and A. L. N. Moreira, "Bubble dynamics and heat transfer on biphilic surfaces," in Proceedings of the 16th UK Heat Transfer Conference (UKHTC2019), p. 3., 2019.